INTERNATIONAL JOURNAL OF Telecommunications AIR DEFENSE COLLEGE

Fast Convergence Modified Particle Swarm Optimization Algorithm to Follow up String PV Modules Maximum Power Point under Different Climatic Conditions

Ehab Mohamed Ali[1,*], Ahmed K. Abdelsalam[2] and Ahmed A. Hossam-Eldin[3]

Citation: Ali, E. M.; Abdelsalam, A. K.; Hossam-Eldin, A. A. *International Journal of Telecommunications*, ***IJT'2021***, *Vol. 01, Issue 01, pp. 1-16, December 2021*. https://ijt-adc.org/articles/2805-3044/109361

Editor-in-Chief: Yasser M. Madany

Received: 30-10-2021

Accepted: 1-12-2021

Published: 18-12-2021

Publisher's Note: The International Journal of Telecommunications, IJT, stays neutral regarding jurisdictional claims in published maps and institutional affiliations.

[1] Air Defense College, Alexandria University, Alexandria, Egypt; ehab.ali.7510m.adc@alexu.edu.eg

[2] Electrical Engineering Department, Arab Academy for Science and Technology & Maritime Transport, Alexandria, Egypt; ahmed.kadry@aast.edu

[3] Electrical Engineering Department, Faculty of Engineering, Alexandria University, Alexandria, Egypt; a.hossamudn@alexu.edu.eg

* Correspondence: ehab.ali.7510m.adc@alexu.edu.eg.

Abstract: Photovoltaics are extensively used as a premium device for generating electricity from solar planet's power. Under uniform radiation, the photovoltaics' output characteristics have a non-linear frame with a unique maximum power point. This point changes its position when a sudden change in solar radiation occurs. Otherwise, when the PV string is subjected to partial shading conditions, several power peaks have appeared with only one Global maximum power. The classical maximum power point tracking strategies always fails to deal with these dynamic difficulties, especially, under unexpected climatic changes. Many soft computing methods are previously constructed to deal with these problems, but the main hurdles remain how to manage this tracking with the fastest time, the smallest power oscillations, and the greatest efficiency. In this paper, a modified Particle Swarm Optimization algorithm was proposed that capable of excluding or promoting certain parts of the solution search area until reach and track the max power point. The suggested method has been simulated and practically tested and the results indicate that the suggested method outperforms the typical Particle Swarm Optimization algorithm with regards to the speed of Global maximum power point tracking with the lowest oscillation and highest efficiency.

Keywords: Maximum Power Point Tracking (MPPT); Photovoltaic (PV); Partial Shading (PS); Particle Swarm Optimization (PSO); Global Maximum Power Point (GMPP).

1. Introduction

Lately, electric power generation using photovoltaic (PV) technology has received great consideration to meet the extreme power requirement. Furthermore, it is considered a favored technology because it works without any pollution, is free maintenance, and environmentally friendly. The PV cells can transform the solar radiation into a certain amount of direct current (DC) electricity. This amount of electricity can be increased by interconnected collection of PV cells to form a module. Several modules can be connected in series or parallel or both to form a PV array. by that the larger the area of PV cells connection, the more DC electricity can be produced [1].

The PV cell's output properties are non-linear and simply affected by the variation in the solar radiation and the enclosing temperature. This output property can be portrayed by the PV output power against the PV output voltage that is named the P-V curve of the PV cells. This curve has only one power peak in the case of Uniform Solar Radiation (USR) as shown in Figure 1 (a) [2].

On the other hand, it has several power peaks in the case of Partial Shading Conditions (PSC) one of them is the Global Maximum Power Point (GMPP) as shown in Figure 1 (b) [3]. These several power peaks formed according to connecting the bypass diodes in parallel with the PV cells to avoid hotspot problems. In this case, the excess current over the short circuit current value of the shaded PV cell can be passing through the bypass diode and leads to form numerous power peaks in the P-V curve [4].
So, Max Power Point Tracking (MPPT) controller is considered as a required part for the PV system to assure that the system is operated at the maximum available output power of the PV string. All the controllers are depending on estimating a number of duty cycles samples that are fed one by one to the interface converter's switch to change the total impedance seen by the PV string. This estimation depends on the controller's strategy, and it stopped when the PV system operating point reaches the GMPP. The overall PV system can be displayed in Figure 2. [5].

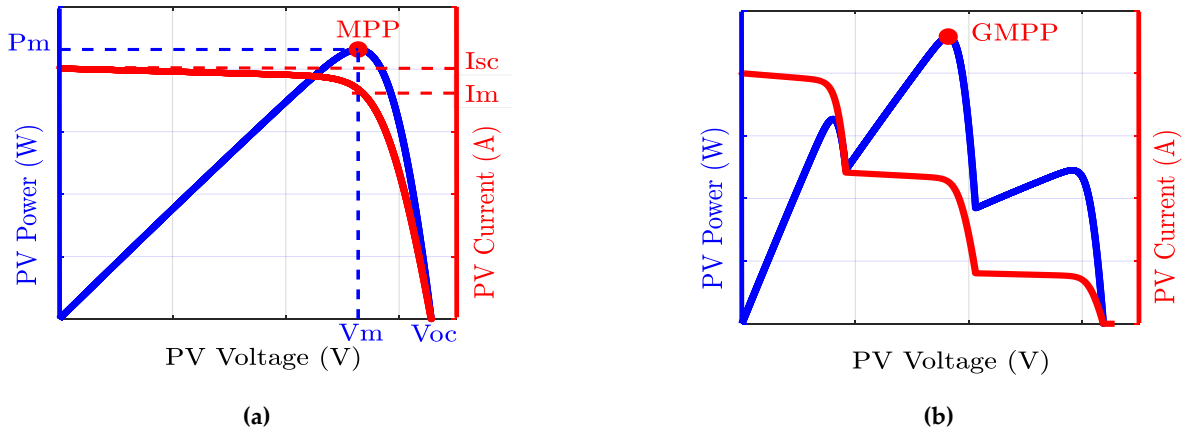

Figure 1. The PV string's power-against-voltage curve and current- against-voltage curve (a) under USR (b) under PSC.

Various traditional MPPT controllers have been developed and successfully deal with tracking the unique maximum power peak formed during the USR conditions. These controllers are differing in their implementation cost, the number of required sensors, and their algorithm complexity. But still, their main objective is how to achieve fast and accurate tracking with minimum power oscillations. These controllers such as Fractional Short Circuit Current (FSC), Fractional Open-Circuit voltage (FOC), Incremental Conductance method (IC), and Perturb & Observe method (P&O) [6].

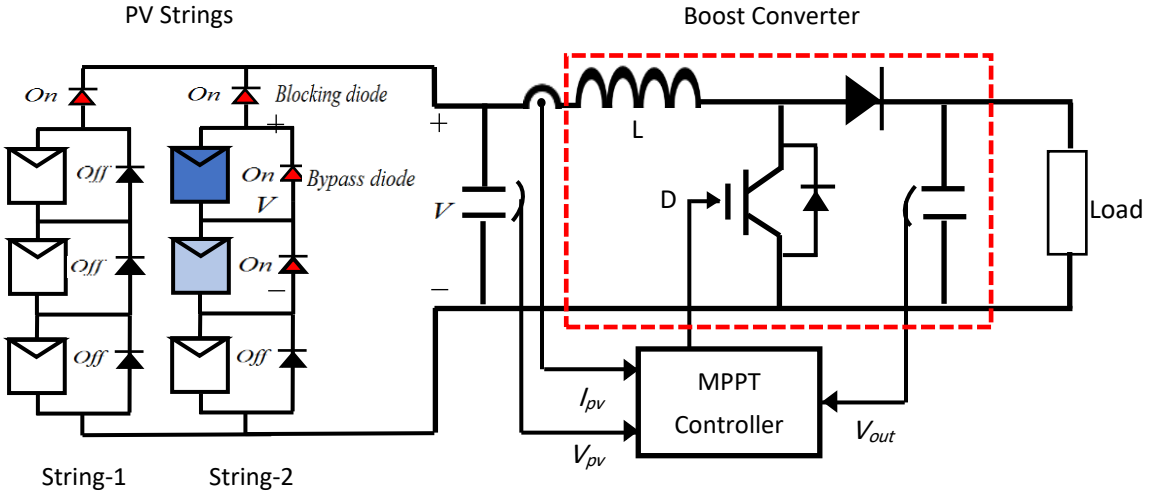

Figure 2. The whole PV system with two PV strings subjected to different radiation conditions.

In the case of PSC, the traditional MPPT controllers fail to differentiate between the Global Max Power Point (GMPP) and the Local Maximum Power Points (LMPP). That leads to let the controller track the first power peak it will reach. This problem is dissolved by utilizing Artificial Intelligence (AI), and meta-heuristic con-

trollers [7]. The MPPT controllers that are based on AI algorithms operate effectively than the traditional ones, but it needed extra sensors to sense the radiation and temperature variation, also it requires significant memory to store a great amount of data and requires previous knowledge about the PV system. For example, the Artificial Neural Network (ANN) controller, and the Fuzzy Logic Control (FLC) [8].

The meta-heuristic controllers are beating both Artificial Intelligence and traditional controllers. It did not need any earlier information about the PV system parameters, the duty cycles (the controller particles) convergence did not want a complicated controller to adjust the step size and the new searching direction for the newly generated particles, and no big storage memory is wanted [9]. But it needs tuning parameters according to the strategy of the controller. This tuning usually depends upon the trial-and-error process. Also, it may repeat the exploration of the area that explored in one of the controller's earlier iterations which increases the tracking time. These controllers including, Simulated Annealing (SA), Ant Colony Optimization (ACO) controller, and Cuckoo Search Algorithm (CSA) [10, 11].

Additionally, hybrid techniques such as, an Overall Distribution (OD) controller to fast exploration the region near GMPP is advanced, which is further joined with Particle Swarm Optimization controller (PSO) to improve the MPPT accuracy [12]. A natural cubic-Spline-guided Jaya (S-Jaya) controller is presented in [13], it is utilized in the iterative update process of the Jaya controller to provide fitting varieties of renewing solutions. Also, the Gray Wolf Optimization (GWO) controller has been joined with the P&O controller in [14]. That joining process leads to enhance the optimization capability, but it increases the complexity of the controller implementation.

In extension to the earlier controllers, the Particle Swarm Optimization (PSO) controller was ranked as a meta-heuristic algorithm. This controller is relying on the communicative behavior of bird swarms and fish schools. It predicates on the exploration in a random way and the use of earlier results to improve the next exploration process in the search space. Notwithstanding, the PSO controller's efficiency required improvement, and its convergence manner creates high transient oscillation [15].

The principal contribution of this paper is to modify the performance of the PSO controller base MPPT in terms of its capacity to explore as well as exploit the search area. It aims to decrease the search area limits after each iteration. The proposed improved PSO (IPSO) controller generates new particles samples to explore the area inside these renewed limits. Consequently, it compensates for the time wasted due to the random steps and reduces the power oscillation in the transient state.

2. Materials and Methods

2.1. The mathematical modeling and performance of the solar PV module

The PV cell's constructed material is a p-n junction manufactured in a thin wafer of semiconductors. It can be modeled by using an equivalent circuit to help control its performance and characteristics in the labor experimental [16].

2.1.1. The PV string under USR

There are three PV modules are joined together in a series connection to form string-1 as shown in Figure 2. These PV modules are received the same solar radiation at the same time and act as a forward-biased semiconductor device that leads to passing the same current value through the PV string. On the other hand, the bypass diodes act as a reverse-biased semiconductor device without passing any current through it [17].

The one diode model is widely used as a PV module equivalent circuit. This circuit consisted of a photocurrent source, diode, a shunt resistor, and a series resistor as shown in Figure 3 (a). The characteristics equation of the PV module output current can be given as [18]:

$$I_{Pv} = I_{Ph} - I_D - I_{sh} \tag{1}$$

Then,

$$I_{Pv} = \left[[I_{sc} + K_i(T - T_r)] \times \frac{\lambda}{1000} \right] - \left[I_s \times \left(e^{\frac{q\left(\frac{V}{N_s} + \frac{IR_s}{N_p}\right)}{AKT}} - 1 \right) \right] - \left[N_p \times \frac{\left(\frac{V}{N_s} + \frac{IR_s}{N_p}\right)}{R_{sh}} \right] \tag{2}$$

The diode saturation current can be calculated by:

$$I_s = I_{rs} \times \left(\frac{T}{T_r}\right)^3 \times e^{\frac{qE_g\left(\frac{1}{T_r}-\frac{1}{T}\right)}{AK}} \quad (3)$$

The cell reverse saturation current can be calculated by:

$$I_{rs} = \frac{I_{sc}}{\left[e^{\frac{qV_{oc}}{AN_sKT_r}} - 1\right]} \quad (4)$$

Where the equation's symbols can be defined as listed in Table.1.

Table 1. The characteristics equation's parameters of the PV module output current [18].

The symbol	The definition
I_{sc}	the PV short circuit current at reference radiation and temperature
K_i	the short circuit current temp coefficient
T	the absolute temperature of the PV cell
T_r	the reference temperature (298 Kelvin)
λ	the solar radiation in (W/m^2)
I_s	the diode saturation current
q	the electron charge $= (1.602 \times 10^{-19}\ J/V)$
N_s	the number of series PV cells in the module
N_p	the number of parallel PV cells in the module
A	the diode ideality factor
K	the Boltzmann constant $= (1.381 \times 10^{-23}\ J/K)$
I_{rs}	the cell reverse saturation current
E_g	the bandgap energy $= (1.1\ eV)$
V_{oc}	the open-circuit voltage of the PV cell
R_{sh}	the internal shunt resistance of the PV cell
R_s	the internal series resistance of the PV cell

2.1.2. The PV string under PSC

There are three PV modules are joined together in a series connection to form string-2 as shown in Figure 2. These PV modules are partially shaded and received different solar radiation at the same time. The short circuit current of the shaded PV modules breaks to zero and these modules act as a reverse-biased semiconductor device. A negative voltage drop can be formed across the shaded PV modules due to the non-shaded PV module's current which leads to forming a hotspot at the shaded location. This hotspot reduced the module efficiency and shortened its lifetime. The opposite polarity bypass diode can be preventing the shaded PV modules from the hotspot when it is connected in parallel with it. It works as a forward-biased semiconductor device which leads to passing the excess current of the non-shaded PV module through it. This operation leads to change the P-V curve characteristics in terms of formed multiple power peaks. These partially shaded modules can be expressed by the equivalent circuit in Figure 3 (b) [19].

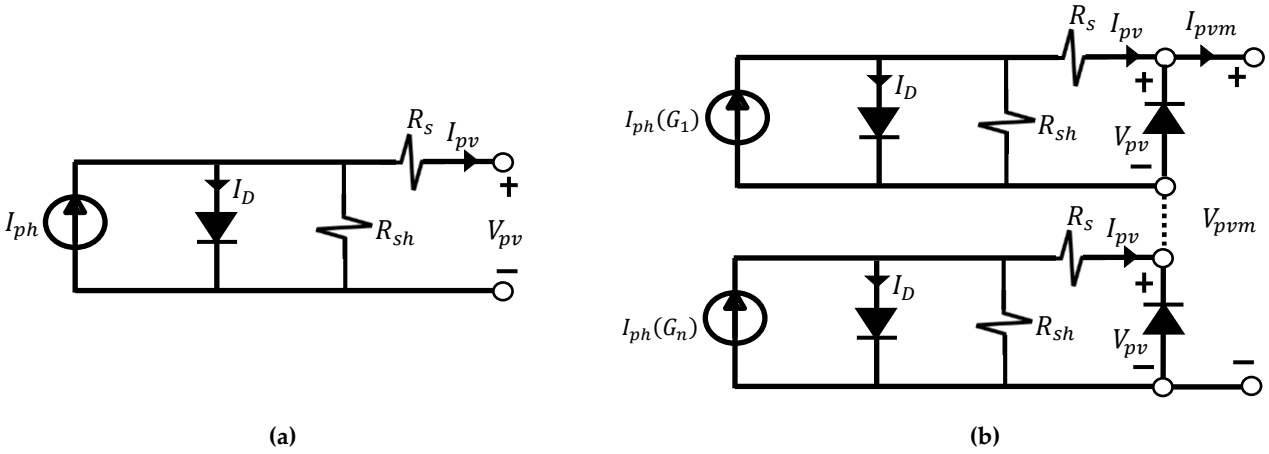

Figure 3. The PV module's equivalent circuit (a) under USR (b) under PSC

2.2. The PSO Idea and its Implementation for PV String's MPPT Controller

2.2.1. The Main Idea of the PSO algorithm

Eberhart and Kennedy introduced a Global optimization algorithm called the PSO algorithm in 1995 [20]. Lately, this algorithm has been successfully employed to solve several engineering applications problems. The bird's swarm's behavior in terms of exploring for food and picking the most fitting place to live are the primary concepts that were employed for establishing that algorithm.

To explain, in the PSO algorithm, the individuals that live in the bird's swarm are named particles. At the start of the exploration process, each particle is spread in various places with various speeds without disrupting the interaction between them. That interaction allows them to modernize the swarm global best position systematically. On the other hand, each particle has its individual best position. In that way, each particle is excited to a fresh position after modernizing its velocity and direction. This modernizing process is affected by three manners called the swarm Global best position, the personal best position, and the trend to random exploration. The exploration process is continuing by beneficial the earlier experiences for both the individual and the swarm till all particles arrive at the optimum position (optimum solution) [21].

2.2.2. The PSO algorithm as a Candidate for MPPT controller in the PV systems

The PSO algorithm is employed in order to use its strategy to generate the duty cycles samples (dc_i^t) (particles). The symbol (dc_i^t) upper and lower subscripts indicate the iterations number (t) and the duty cycle number (i) respectively. These duty cycles samples can be estimated by feeding one by one to the PV system's converter and in each case, the outputs are measured. The algorithm parameters are adjusted to match the PV system characteristics. This adjustment process included the swarm-acceleration coefficient (α) that set to a value between 2 and 2.5, the inertia weight (θ) which set to 0.5, and the self-acceleration coefficient (β) that set to a value between 1.5 and 2 [22].

The PSO algorithm based MPPT designer chooses the population size of (n) random duty cycle samples among the standard duty cycles values between 0 and1. These samples were used to trigger the PV system converter's switch. For each sample, the PV output voltage and current are measured, and by multiplying these values the output power can be calculated and stored. After each iteration, each particle updates its velocity v_i^{t+1} and position dc_i^{t+1} by using equations 5, and 6, respectively. The new power values are calculated and compared with the previous values to identify the particle's personal best value dc_{i_best} and the Global best duty cycle sample dc_{Gbest} for the next iterations.

$$v_i^{t+1} = \theta v_i^t + \alpha\epsilon_1(dc_{Gbest} - dc_i^t) + \beta\epsilon_2(dc_{i\_best} - dc_i^t) \quad (5)$$

$$dc_i^{t+1} = dc_i^t + v_i^{t+1} \quad (6)$$

The algorithm stopped its iterations when all duty cycles samples reach the GMPP.

2.3. The Proposed Improved PSO (IPSO) Controller Performance

Consequently, an authoritative study was achieved for various P-V curves which involved diverse locations for GMPP. After this study, remarkable outcomes that can support the PSO controller to track the GMPP in minimum possible time and with high accuracy were reached. These outcomes can be correctly achieved when the controller starts its exploration with evenly distributed duty cycles samples between 0 and 1. Also, the proposed controller satisfied with only five duty cycles samples for the exploration process. This start gives a hypothetical representation of the P-V curve. Then, the recorded outcomes aided the algorithm to reduce the exploration area after each iteration. The IPSO controller's performance can be organized in the flowchart that showed in Figure 5 and arranged in the following steps:

In step 1, the proposed controller initializes five evenly distributed samples of duty cycles to cover the entire P-V curve. These samples are equal to, $\mathrm{dc}_1^1 = 0.1$, $\mathrm{dc}_2^1 = 0.3$, $\mathrm{dc}_3^1 = 0.5$, $\mathrm{dc}_4^1 = 0.7$ and $\mathrm{dc}_5^1 = 0.9$. Also, the algorithm set the Global best position to $dc_{\mathrm{Gbest}}^1 = 0$, and the personal best position $dc_{\mathrm{i-best}}^1 = 0$, and $\mathrm{dc}_{\mathrm{i}}^{\mathrm{t}} = [0, 1]$.

In step 2, the proposed controller estimates each sample across the PV system's converter switch, and the sample's operating point data were stored in a matrix. This data is specified by the values of duty cycle, the output voltage, and the output current.

In step 3, the proposed controller multiplied the stored PV output voltage and current to obtain the PV output power value for each sample.

In step 4, the proposed controller re-specified the Global best sample which achieves the maximum stored power value $\mathrm{P_{max}}$ at the end of each iteration.

In step 5, the proposed controller re-specified the personal best position for each sample in all the previous iterations till now.

In step 6, the proposed controller arranged the stores matrix's rows according to the voltage values in descending order. After this arrangement process, the algorithm symbolizes the matrix's rows as A, B, C, D, and E.

In step 7, the power value of the stored matrix's row "C" is becoming the power corresponding to the middle voltage value located on the P-V curve for the present iteration. So, this power value is chosen to be the reference power value in this iteration. This reference power value divided the exploration space into two different exploration area located in its both sides.

In step 8, the reference power value is compared with the other power values in the same iteration to visualize the look of the exploration area. This comparing process can be groups into three main cases as following:

- The reference power value is higher than the other two power values who are on its each side separately:

In this case, the reliability of located the GMPP around the reference power location is higher than its location around the lesser power values. So, the proposed controller eliminates the area between the lesser power values and sets the new exploration area's boundaries to be between the reference power value and the nearest power value as described in Table 2.

- The reference power value has a value between the other two power values:

In this case, the proposed controller advances the area between the highest power value and the reference power value to be the new exploration area for the next iteration as explained in Table 3.

- The reference power value is lower than the other two power values who are on its each side separately:

In this case, the proposed controller is forced to search again inside the all-search area without eliminates any part of it as described in Table 4.

In step 9, the proposed controller generates new duty cycles samples and chick if any of that new samples are located outside the new boundaries of the exploration area or not. If the chick is true, the algorithm chooses the duty cycle value that located between the previous two highest stored power values $dc(P_{max1}), and\ dc(P_{max2})$ respectively. That can be achieved by using equation (7).

$$dc_{New} = dc(P_{max2}) + \frac{dc(P_{max1}) - dc(P_{max2})}{2} \tag{7}$$

In step 10, the proposed controller estimates the new generated samples and calculates the output power values. The algorithm chick if all the duty cycles samples reached the GMPP or not. If false, the algorithm returns to step number four and repeat the next steps again. If true, the algorithm stopped its operation.

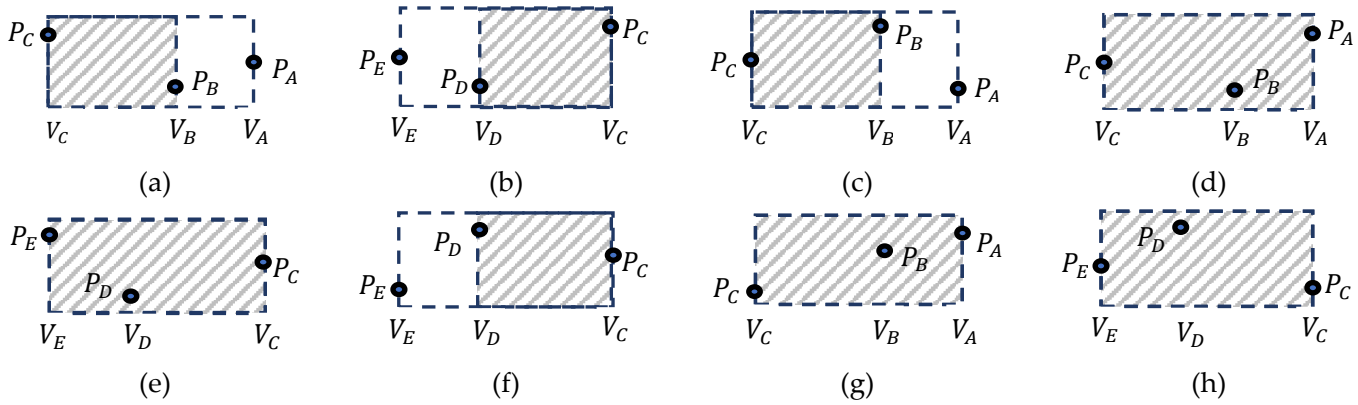

Figure 4. The feature of the proposed (IPSO) algorithm's supported conditions.

Table 2. The first case of the proposed (IPSO) algorithm's supported conditions.

"Check If circumstance"	**Recent boundaries of the exploration space**		**the design explanation**
	from	***To***	
The reference power value's right side			
$p_C(dc_i^t) > p_A(dc_i^t), p_B(dc_i^t)$	$v_B(dc_i^t)$	$v_C(dc_i^t)$	Figure 4 (a)
The reference power value's left side			
$p_C(dc_i^t) > p_D(dc_i^t), p_E(dc_i^t)$	$v_C(dc_i^t)$	$v_D(dc_i^t)$	Figure 4 (b)

Table 3. The second case of the proposed (IPSO) algorithm's supported conditions.

"Check If circumstance"	**Recent boundaries of the exploration space**		**the design explanation**
	from	***To***	
The reference power value's right side			
$p_C(dc_i^t) > p_A(dc_i^t)$ & $p_C(dc_i^t) < p_B(dc_i^t)$	$v_B(dc_i^t)$	$v_C(dc_i^t)$	Figure 4 (c)
$p_C(dc_i^t) < p_A(dc_i^t)$ & $p_C(dc_i^t) > p_B(dc_i^t)$	$v_A(dc_i^t)$		Figure 4 (d)
The reference power value's left side			
$p_C(dc_i^t) > p_D(dc_i^t)$ & $p_C(dc_i^t) < p_E(dc_i^t)$	$v_C(dc_i^t)$	$v_E(dc_i^t)$	Figure 4 (e)
$p_C(dc_i^t) < p_D(dc_i^t)$ & $p_C(dc_i^t) > p_E(dc_i^t)$		$v_D(dc_i^t)$	Figure 4 (f)

Table 4. The third case of the proposed (IPSO) algorithm's supported conditions.

"Check If circumstance"	**Recent boundaries of the exploration space**		**the design explanation**
	from	***To***	
The reference power value's right side			
$p_C(dc_i^t) < p_A(dc_i^t), p_B(dc_i^t)$	$v_A(dc_i^t)$	$v_C(dc_i^t)$	Figure 4 (g)
The reference power value's left side			
$p_C(dc_i^t) < p_D(dc_i^t), p_E(dc_i^t)$	$v_C(dc_i^t)$	$v_E(dc_i^t)$	Figure 4 (h)

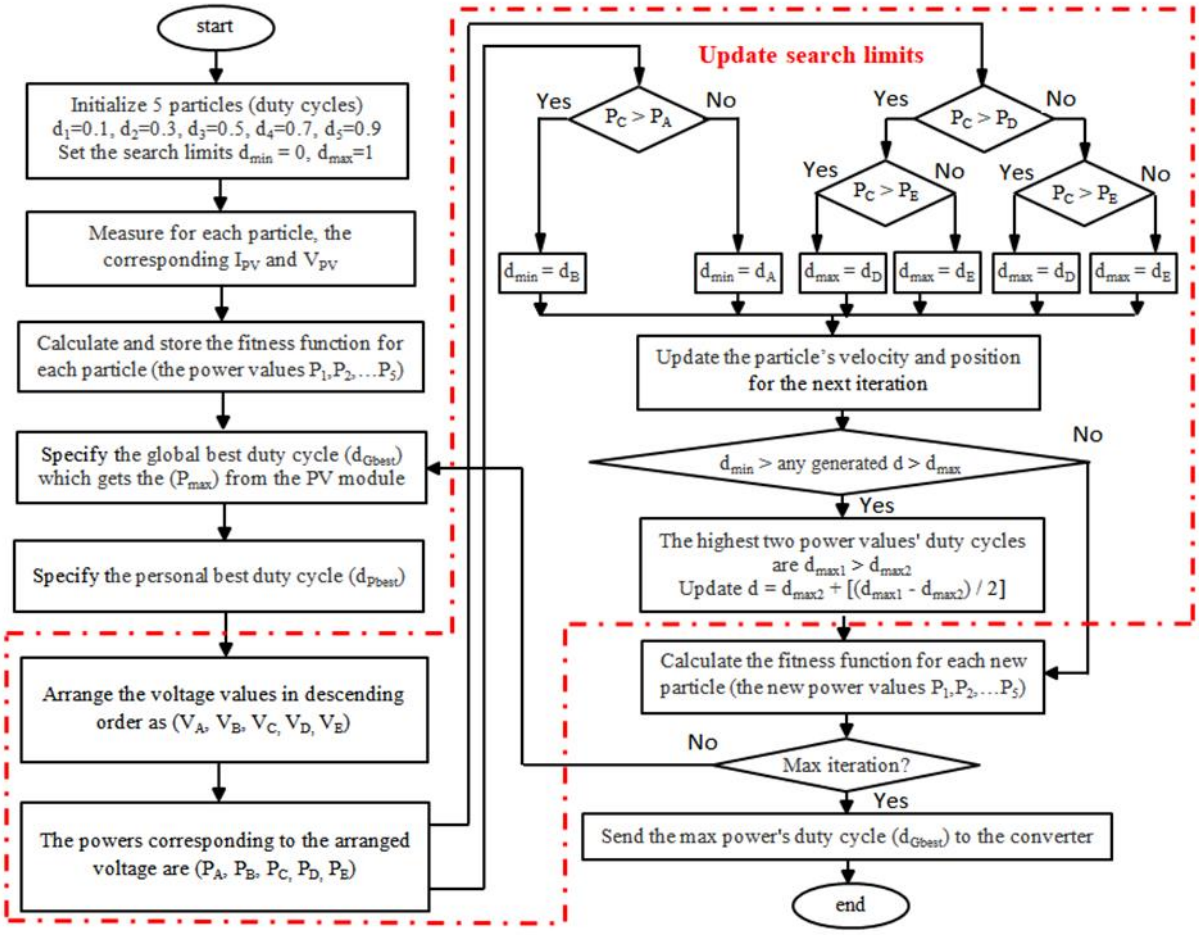

Figure 5. The sequence of operation's diagram for the proposed (IPSO) algorithm

3. Results

3.1. The Simulation Results

The proposed IPSO algorithm was simulated and tested by using Matlab/Simulink program. This simulated program helps in comparing the performance of both the proposed and the classical PSO controllers in terms of the transient and the steady-state waveform. It also shows the first four iterations for the proposed IPSO controller performance in terms of decreasing the exploration area after each iteration and catches the GMPP.

The PV system that is designed and simulated in the Matlab/Simulink program can be controlled by using a different number of PV modules. On the other hand, the solar radiation value can be controlled to simulate the USR, the PSC, and the sudden change in solar radiation. The parameters of the simulated PV system's PV modules and boost converter are listed in Table 5.

Table 5. The parameters of the Matlab / Simulink pattern.

PV module	Values	Boost converter	Values
Short circuit current I_{sc}	8.02A	The input capacitor C_{in}	10μF
Open circuit voltage V_o	21.9V	The converter inductor L	1.1mH
Voltage at max power point V_m	17.6V	The switch frequency f	50kHz
Current at max power point I_m	7.39A	The output capacitor C_{out}	0.5mF

3.1.1. The PV system subjected to USR (shape # 1)

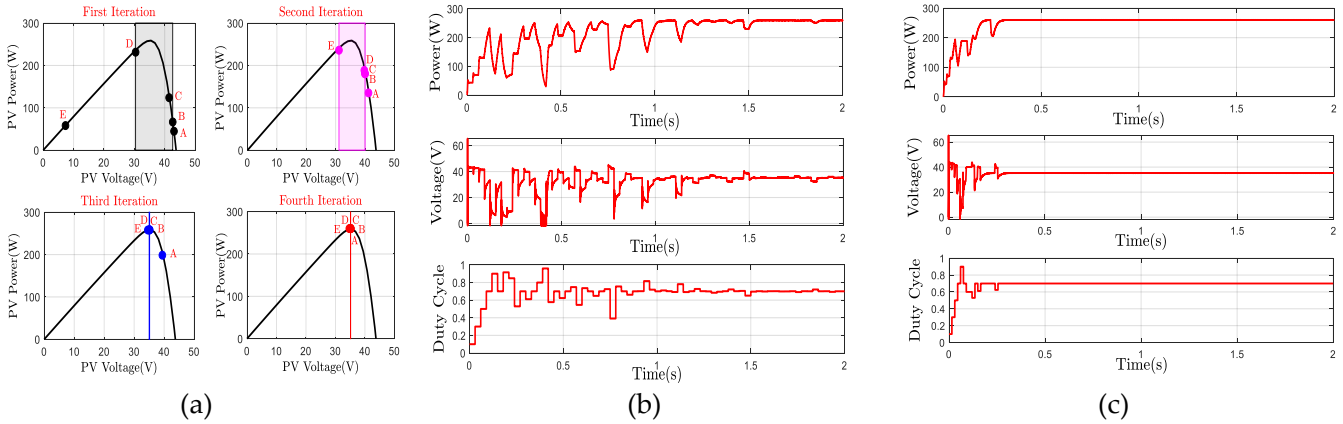

Figure 6. The tracking process for shape # 1. (a) The proposed controller's retraction process toward the MPP. (b) The tracking trajectory in the case of the classical PSO controller. (c) The tracking trajectory in the case of the proposed IPSO controller.

Table 6. The first four iterations' stored data for the proposed IPSO controller performance during estimated shape # 1.

Row	n	The first iteration			n	The second iteration			n	The third iteration			n	The fourth iteration		
		dc	V_{PV} *(V)*	P_{PV} *(W)*		*dc*	V_{PV} *(V)*	P_{PV} *(W)*		*dc*	V_{PV} *(V)*	P_{PV} *(W)*		*dc*	V_{PV} *(V)*	P_{PV} *(W)*
A	dc_1^1	0.1	43.06	44.68	dc_3^2	0.52	41.19	135.2	dc_5^3	0.62	39.41	198.57	dc_5^4	0.7	35.2	260
B	dc_2^1	0.3	42.64	66.58	dc_2^2	0.6	40	180.43	dc_4^3	0.7	35.18	258.36	dc_4^4	0.7	35.19	260
C	dc_3^1	0.5	41.45	123.93	dc_1^2	0.6	40	180.44	dc_3^3	0.7	35.14	258.38	dc_3^4	0.7	35.15	260
D	dc_4^1	0.7	30.42	231.34	dc_5^2	0.61	39.76	188.47	dc_2^3	0.7	35	258.39	dc_2^4	0.7	35.04	260
E	dc_5^1	0.9	7.33	58.04	dc_4^2	0.7	31.13	236	dc_1^3	0.7	34.57	258	dc_1^4	0.7	34.7	260

3.1.2. The PV system subjected to PSC (shape # 2, 3, and 4)

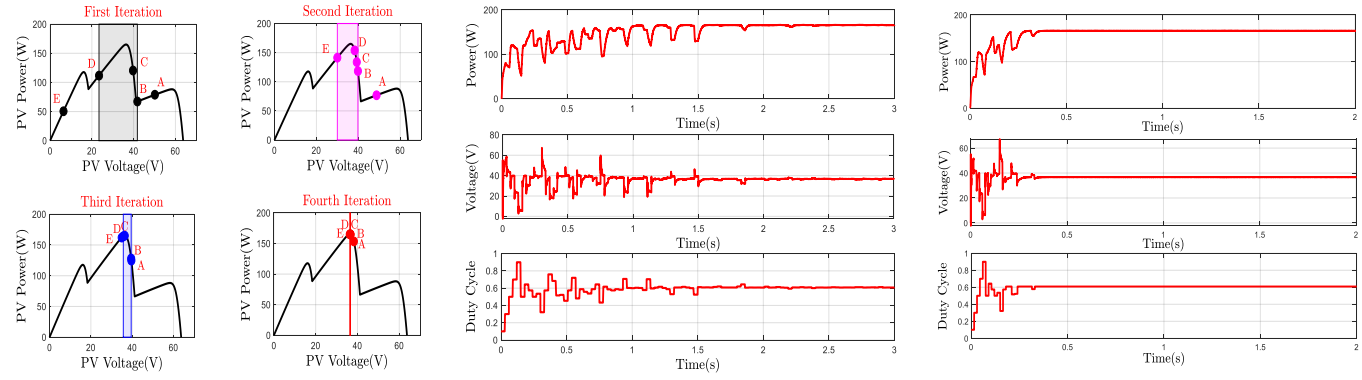

Figure 7. The tracking process for shape # 2. (a) The proposed controller's retraction process toward the GMPP. (b) The tracking trajectory in the case of the classical PSO controller. (c) The tracking trajectory in the case of the proposed IPSO controller.

Table 7. The first four iterations' stored data for the proposed IPSO controller performance during estimated shape # 2.

Row	n	The first iteration			n	The second iteration			n	The third iteration			n	The fourth iteration		
		dc	V_{PV} *(V)*	P_{PV} *(W)*		*dc*	V_{PV} *(V)*	P_{PV} *(W)*		*dc*	V_{PV} *(V)*	P_{PV} *(W)*		*dc*	V_{PV} *(V)*	P_{PV} *(W)*
A	dc_1^1	0.1	50.87	78.35	dc_5^2	0.32	48.71	76.81	dc_3^3	0.51	39.61	124.6	dc_4^4	0.57	38.28	153.4
B	dc_2^1	0.3	41.77	62.53	dc_3^2	0.5	39.83	118.4	dc_4^3	0.52	39.51	128	dc_3^4	0.61	36.68	164.8
C	dc_3^1	0.5	39.84	112.57	dc_4^2	0.53	39.28	133.8	dc_2^3	0.61	36.40	165	dc_2^4	0.61	36.65	164.8

Row	n	The first iteration			n	The second iteration			n	The third iteration			n	The fourth iteration		
		dc	V_{PV} *(V)*	P_{PV} *(W)*		*dc*	V_{PV} *(V)*	P_{PV} *(W)*		*dc*	V_{PV} *(V)*	P_{PV} *(W)*		*dc*	V_{PV} *(V)*	P_{PV} *(W)*
D	dc_4^1	0.7	23.42	108.75	dc_2^2	0.57	38.24	153.9	dc_1^3	0.61	35.69	164.2	dc_1^4	0.61	36.53	165
E	dc_5^1	0.9	6.16	48.5	dc_1^2	0.64	29.99	141.3	dc_5^3	0.61	34.92	162	dc_5^4	0.61	36.31	165

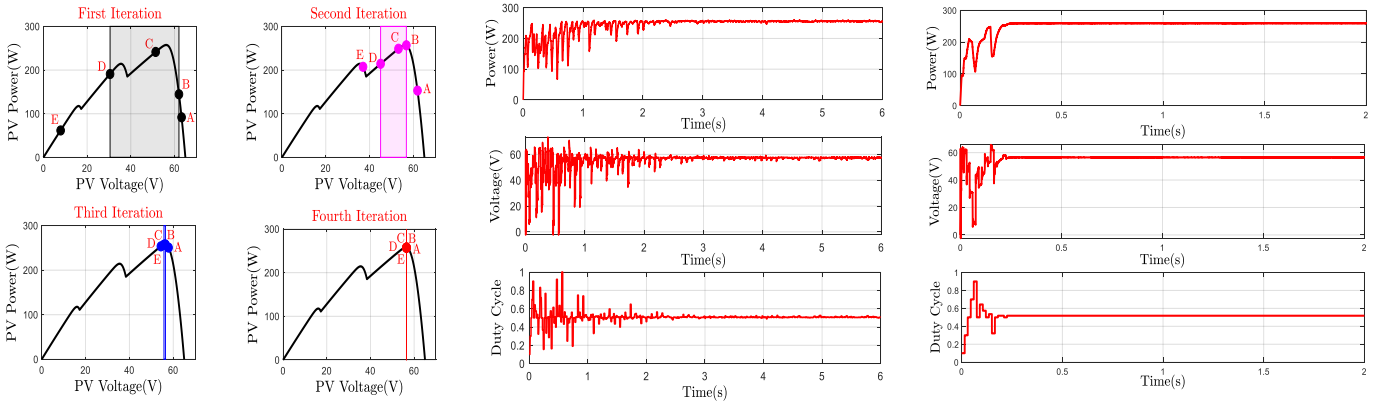

(a) (b) (c)

Figure 8. The tracking process for shape # 3. (a) The proposed controller's retraction process toward the GMPP. (b) The tracking trajectory in the case of the classical PSO controller. (c) The tracking trajectory in the case of the proposed IPSO controller.

Table 8. The first four iterations' stored data for the proposed IPSO controller performance during estimated shape # 3.

Row	n	The first iteration			n	The second iteration			n	The third iteration			n	The fourth iteration		
		dc	V_{PV} *(V)*	P_{PV} *(W)*		*dc*	V_{PV} *(V)*	P_{PV} *(W)*		*dc*	V_{PV} *(V)*	P_{PV} *(W)*		*dc*	V_{PV} *(V)*	P_{PV} *(W)*
A	dc_1^1	0.1	63.31	89.25	dc_5^2	0.32	61.85	153	dc_3^3	0.5	57.86	250.6	dc_5^4	0.52	56.503	257.3
B	dc_2^1	0.3	62.05	138.24	dc_3^2	0.5	56.76	256.8	dc_5^3	0.52	56.45	257.4	dc_4^4	0.52	56.503	257.3
C	dc_3^1	0.5	52.67	236.07	dc_4^2	0.53	53.17	248.9	dc_4^3	0.52	56.29	257.5	dc_3^4	0.52	56.502	257.3
D	dc_4^1	0.7	30.85	188.19	dc_2^2	0.57	45.01	214.4	dc_2^3	0.52	55.76	257.2	dc_2^4	0.52	56.501	257.3
E	dc_5^1	0.9	7.5	58.93	dc_1^2	0.64	37.1	207.5	dc_1^3	0.52	54.36	253.4	dc_1^4	0.52	56.490	257.3

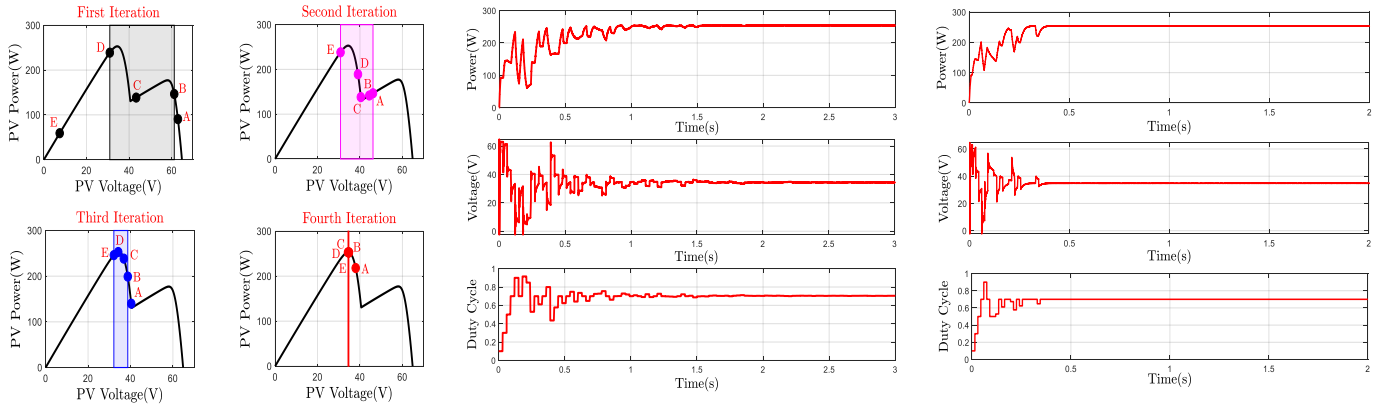

(a) (b) (c)

Figure 9. The tracking process for shape # 4. (a) The proposed controller's retraction process toward the GMPP. (b) The tracking trajectory in the case of the classical PSO controller. (c) The tracking trajectory in the case of the proposed IPSO controller.

Table 9. The first four iterations' stored data for the proposed IPSO controller performance during estimated shape # 4.

Row	n	The first iteration			n	The second iteration			n	The third iteration			n	The fourth iteration		
		dc	V_{PV} *(V)*	P_{PV} *(W)*		*dc*	V_{PV} *(V)*	P_{PV} *(W)*		*dc*	V_{PV} *(V)*	P_{PV} *(W)*		*dc*	V_{PV} *(V)*	P_{PV} *(W)*
A	dc_1^1	0.1	62.933	90.5	dc_1^2	0.5	46.139	146.7	dc_3^3	0.58	40.36	139.8	dc_5^4	0.64	37.98	218.1
B	dc_2^1	0.3	61.214	146.6	dc_2^2	0.5	44.393	141.7	dc_5^3	0.62	38.73	199.1	dc_4^4	0.7	34.77	252.7
C	dc_3^1	0.5	43.322	138.6	dc_3^2	0.52	40.402	138.1	dc_2^3	0.67	36.86	238.4	dc_3^4	0.7	34.75	252.8
D	dc_4^1	0.7	30.939	238.9	dc_5^2	0.61	39.036	189.1	dc_1^3	0.7	34.238	252.9	dc_2^4	0.7	34.66	252.9
E	dc_5^1	0.9	7.405	58.99	dc_4^2	0.7	30.836	238.2	dc_4^3	0.7	32.17	246.1	dc_1^4	0.7	34.35	253

3.1.3. The PV system subjected to sudden change in solar radiation (shape # 5)

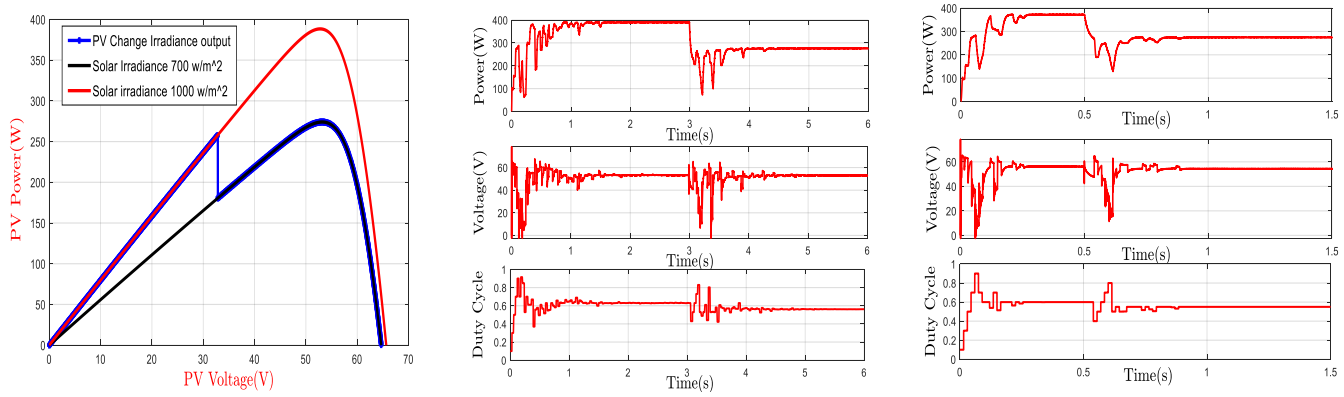

(a) (b) (c)

Figure 10. The tracking process for shape # 5. (a) The proposed controller's retraction process toward the MPP. (b) The tracking trajectory in the case of the classical PSO controller. (c) The tracking trajectory in the case of the proposed IPSO controller.

3.2. The Experemental Results

As a method to authenticate the effectiveness of the proposed IPSO controller, an experimental setup was constructed and tested in the laboratory. The experimental setup consists of, current sensor "LA-55P" to sense the PV output current, voltage sensor "LV-25" to sense the PV output voltage, boost converter with the inductor of "3mH, 7A", capacitor of "2×2200μF, 50V", fast recovery diode of "100V, 10A", and power MOSFET of "100V, 25A", and battery load of "2×12V, 7Ah".

The proposed IPSO controller is coded into a 32-bits, 150MHz code composer studio interface kit type "TMS320F28335". In order to simulate the uncontrollable environmental conditions, a simple PV simulating circuit is used as shown in Figure 11 (a). This circuit consists of a DC power supply of "20V", two parallel resistance each has "5.5Ω", and a series resistance of "1Ω" [23].

When switch S is closed, the total resistance of the simplified PV circuit "which represents the PV internal resistance" is equal to "3.75Ω". According to the max power transfer theorem, Zin = Zl, the max PV output power is transferred to the load when the load resistance is equal to the PV source internal resistance. This matching process occurs when the controller changes the duty cycle value until the load resistance equal to "3.75Ω ". This matching operating point occurs at MPP of "26.7W, 10V, and 2.67A" as shown in Figure 11 (b).

When switch S is opened, the total resistance of the simplified PV circuit is equal to "6.5Ω". The matching process occurs when the load resistance equal to "6.5Ω". Then the matching operating point occurs at MPP of "15.4W, 10V, and 1.54A" as shown in Figure 11 (b) [23]. The total experimental photography is shown in Figure 12.

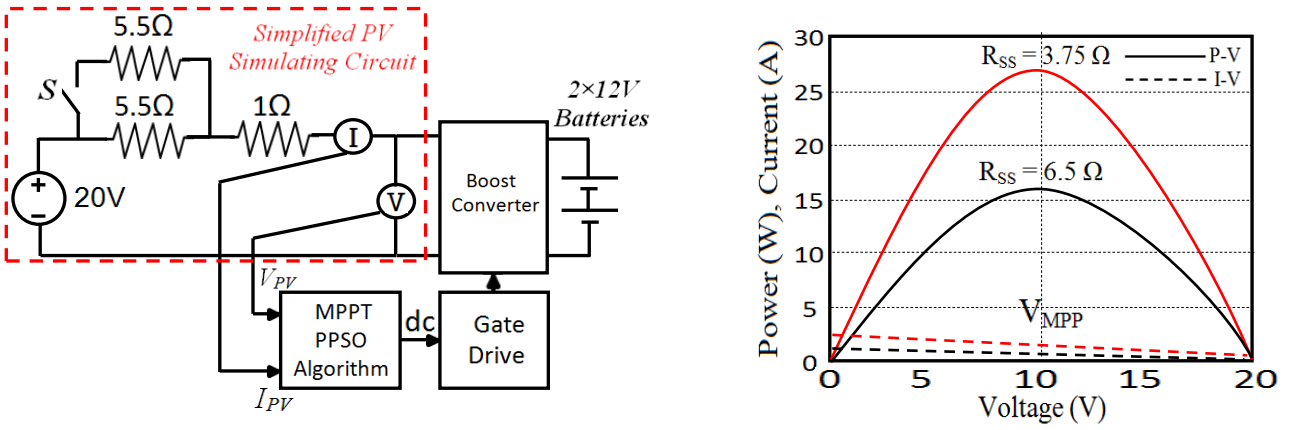

(a) **(b)**

Figure 11. (a) The experimental schematic diagram. (b) The P-V and I-V curves of the simulated PV circuit.

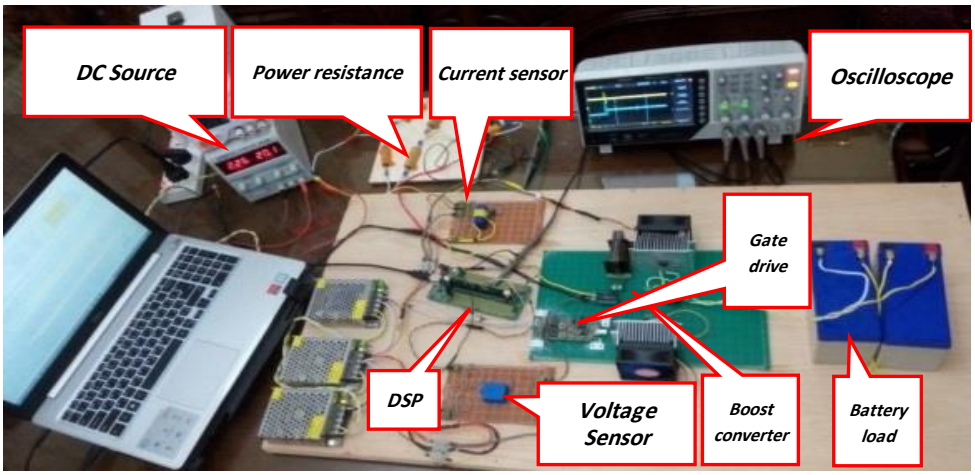

Figure 12. The experimental setup photography

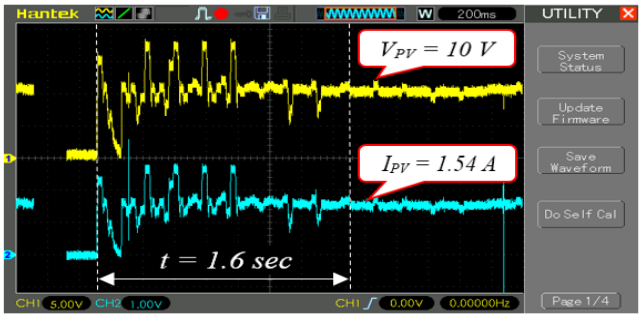

(a)

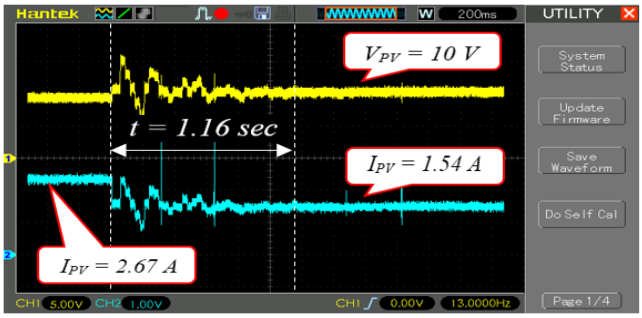

(c)

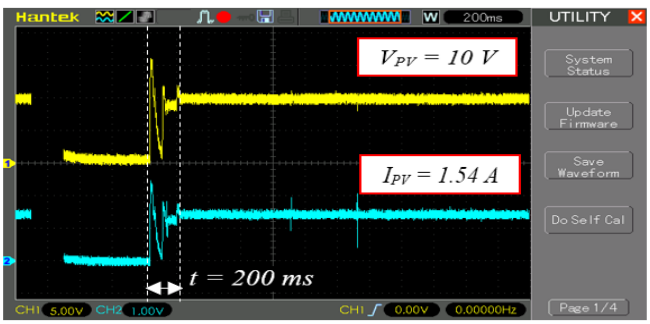

(b)

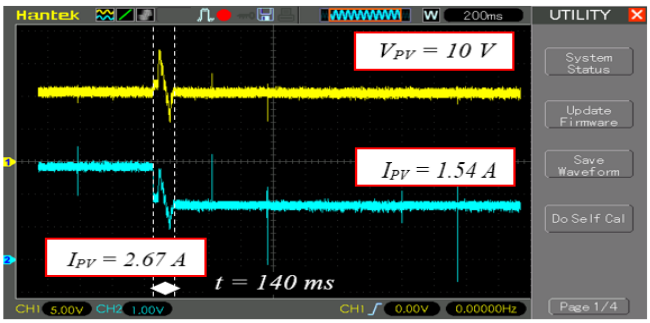

(d)

Figure 13. The experimental results (a) The performance of the classical PSO controller at USR condition (b) The performance of the proposed IPSO controller at USR condition (c) The performance of the classical PSO controller in case of solar radiation change (d) The performance of the proposed IPSO controller in case of solar radiation change.

4. Discussion

4.1. The simulation discussion

Shape # 1 is a PV string containing two PV modules subjected to USR of $1000W/m^2$. The P-V curve of this string has only one power peak of 260W. This shape is estimated twice via Matlab/Simulink, one using the classical PSO controller and the other using the improved IPSO controller. The duty cycles samples' operating points for the first four iterations of the IPSO controller are shown in Figure 6 (a). For each iteration, first, the proposed controller evaluates the duty cycle samples by measuring the PV system output voltage and current and calculating the output power for each duty cycle. The PV system output data "duty cycle, voltage and power" values are rearranged in descending order according to the voltage values. Then, they are stored in a matrix of 3 columns and 5 rows as discussed in the previous section and write down in Table 6. Second, the controller examines the conditions introduced in Figure 4 to determine the new bounders of the exploration area for the next iteration. In the first iteration, the controller found that $p_C(dc_3^1) > p_A(dc_1^1), p_B(dc_2^1)$. Then, the controller sets the voltage value for the matrix's row B $v_B(dc_2^1)$ as the right-hand side border for the new search space. In the same way, $p_C(dc_3^1) < p_D(dc_4^1)$, $p_C(dc_3^1) > p_E(dc_5^1)$ that leads to sets the voltage value for the matrix's row D $v_D(dc_4^1)$ as the left-hand side border for the new search space. In the second iteration, the reference power value is higher than the other two power values on its right side and smaller than the other two power values on its left side. Therefore, the algorithm determined the limits of the new search area to be between the two voltage values $v_B(dc_2^2)$ and $v_E(dc_4^2)$. In the third iteration, the comparison conditions between the reference power value with the rest of the power values were quite similar to the first iteration, and thus the algorithm determined the new search limits to be between the $v_B(dc_4^3)$ and $v_D(dc_2^3)$. In the fourth iteration, all the iteration's power values are equal to the MPP. That's because all the duty cycles are converged until they reached and tracked the MPP. The duty cycles convergence toward the MPP and its corresponding output voltage and power for both the PSO and IPSO controllers are shown in Figures 6 (b) and (c) respectively. It can be observed that the proposed IPSO controller converges toward the MPP of 260W in about 0.35 sec while the classical PSO controller needs about 1.9 sec to follow the MPP.

Shape # 2 is a PV string consisting of three PV partially shaded modules each one has received a different level of irradiance equals to $1000W/m^2$, $600W/m^2$ and $200W/m^2$. Shading in this case resulted in three different peaks of power at 117W, 163W and 88W. For each iteration, first, the controller rearranges and stores the output data in a matrix of 3 columns and 5 rows as recorded in the Table 7. Second, the algorithm examines the conditions introduced in Figure 4 to determine the new bounders of the exploration area for the next iteration. For the first iteration, the controller checks that $p_C(dc_3^1) > p_A(dc_1^1), p_B(dc_2^1)$. As a result, it sets the voltage value for the matrix's row B $v_B(dc_2^1)$ as the right-hand side border for the new search space. In the same way, $p_C(dc_3^1) > p_D(dc_4^1), p_E(dc_5^1)$ leads to sets the voltage value for the matrix's row D $v_D(dc_4^1)$ as the left-hand side border for the new search space. The second iteration check differed from the first one in determining the new left-hand side search limit only and the condition was fulfilled that $p_C(dc_4^2) < p_D(dc_2^2), p_E(dc_1^2)$. So, the result was that the new search area is confined between $v_B(dc_3^2)$ and$v_E(dc_1^2)$. The third iteration check is similar to the first one which leads to let $v_B(dc_4^3)$ and $v_D(dc_1^3)$ are the new right and left search limits respectively. The fourth iteration check is similar to the second iteration which leads to let $v_B(dc_3^4)$ and $v_E(dc_5^4)$ are the new search space limits for the fifth iteration. The positions of the particles in the search area during the first four iterations for the proposed IPSO controller performance are shown in Figure 7 (a). The duty cycle convergence to reach the GMPP is demonstrated in Figures 7 (b) and (c) by using the classical PSO controller and the proposed IPSO controller respectively. These figures indicate that the proposed IPSO controller converges to GMPP of 163W in less than 0.35 sec while the classical PSO controller takes 2.5 sec to track the GMPP with bad fluctuation.

Shape # 3 is a PV string consisting of three PV partially shaded modules each one has received a different level of irradiance equals to $800W/m^2$, $600W/m^2$ and $1000W/m^2$. The shading in this case resulted in three different peaks of power at 117W, 214W and 257W. By the same previous steps, Figure 8 (a) shows the first four iterations for the proposed IPSO controller performance and the data display in the Table 8. The first iteration displays $p_C(dc_3^1) > p_A(dc_1^1), p_B(dc_2^1)$ so that the voltage value for the matrix's row B $v_B(dc_2^1)$ is the right-hand side border for the new search space. Also, the condition $p_C(dc_3^1) > p_D(dc_4^1), p_E(dc_5^1)$ is true and

caused the voltage value for the matrix's row D $v_D(dc_4^1)$ to be the left-hand side border for the new search space. The second iteration check comes true that $p_C(dc_4^2) < p_B(dc_3^2)$, $p_C(dc_4^2) > p_A(dc_5^2), p_D(dc_2^2), p_E(dc_1^2)$ so that the new search area is enclosed between $v_B(dc_3^2)$ and $v_D(dc_2^2)$. The third iteration check is similar to the first one which directs the new search space to be in range within the voltage of sample B $v_B(x_5^3)$ and sample D $v_D(x_2^3)$. The reference power value of the matrix's row C in the fourth iteration is equal to the other four power values. This indicates that all the controller particles have reached the GMPP. The power, voltage and duty cycle curve corresponding to this case is illustrated in Figures 8 (b) and (c) by using the classical PSO controller and the proposed IPSO controller respectively. These graphs indicate that the IPSO controller converges to the GMPP of 257W in less than 0.25 sec while PSO controller takes 2.5 sec to track the GMPP.

Shape # 4 is a PV string consisting of three PV partially shaded modules two of them have received solar irradiance equals to $1000W/m^2$ and the third has received $400W/m^2$. Shading in this case resulted in two different peaks of power at $254W$, and $177W$. Figure 9 (a) shows the first four iterations for the proposed IPSO controller performance, and the data recorded in the Table 9. For the first iteration, the controller makes sure that $p_C(dc_3^1) > p_A(dc_1^1)$ & $p_C(dc_3^1) < p_B(dc_2^1)$. As a result, it sets the voltage value for the matrix's row B $v_B(dc_2^1)$ as the right-hand side border of the new search space. In the same way, $p_C(dc_3^1) < p_D(dc_4^1)$ & $p_C(dc_3^1) > p_E(dc_5^1)$ sets the voltage value for the matrix's row D $v_D(dc_4^1)$ as the left-hand side border of the new search space. The second iteration check differed from the first one and the condition was fulfilled that $p_C(dc_3^2) < p_A(dc_1^2), p_B(dc_2^2)$, and $p_C(dc_3^2) < p_D(dc_5^2), p_E(dc_4^2)$. So that, the new search area is confined between $v_A(dc_1^2)$ and $v_E(dc_4^2)$. In the third iteration, once all the new samples data has been stored, the comparisons with the reference $p_C(dc_2^3)$ prove that $p_C(dc_2^3) > p_A(dc_3^3), p_B(dc_5^3)$ and $p_C(dc_2^3) < p_D(dc_1^3), p_E(dc_4^3)$. The results say that $v_B(dc_5^3)$ and $v_E(dc_4^3)$ are the new search space limits for the fourth iteration. The fourth iteration is similar to the third one. So that, the new search area is confined between $v_B(dc_4^4)$ and $v_E(dc_1^4)$. The duty cycle convergence to reach the GMPP has been illustrated in Figure 9 (b) and Figure 9 (c) by using the classical PSO controller and the proposed IPSO controller respectively. These figures indicate that the IPSO controller converges to the GMPP of 254W in less than 0.4 sec while the PSO controller takes 1.5 sec to track the GMPP.

Shape # 5 is a PV string containing three PV modules subjected to the same solar radiation level equal to $1000W/m^2$. When the solar radiation changes rapidly from $1000W/m^2$ to $700W/m^2$, the MPP's position is changed suddenly, and its value decreases from $370W$ to $275W$ as shown in Figure 10 (a). Both the classical and the suggested PSO controllers have recognized the flickering in solar radiation. So, each controller distributes again its particles to explore and track the new position of the MPP. Figures 10 (b), (c) portray the convergence process for both the classical PSO and the proposed IPSO controllers, respectively. These portray validate the effectiveness of the proposed IPSO controller in terms of taking only 0.4 sec to reach and track the new position of the MPP. While the classical PSO controller takes about 1.3 sec to reach the same point.

4.2. The practical experiment discussion

4.2.1. Uniform Irradiance Condition

The performance of both the classical and the proposed PSO algorithms are tested under uniform environmental conditions. This case can be represented by opening the switch S in the simulated PV circuit.
The performance of the classical PSO algorithm to reach and track the MPP at PV output voltage of"10V" and current of "1.54A" takes about "1.6 sec" with bad fluctuations as shown in Figure 13 (a). While Figure 13 (b) shows that the proposed PSO algorithm takes about "0.2 sec" to reach and track the MPP without any fluctuations at the steady-state condition.

4.2.2. Change the solar irradiance condition

In this case, the position of the MPP is shifted and at this moment the pattern simulates inhomogeneous peaks on the P-V curve. Therefore, MPP tracking becomes more and more difficult. This condition can be represented by sudden closing the switch S in the simulated PV circuit. Before this closing process, the MPP was tracked at "10V, 2.67A, and 26.7W". After that closing process, the controllers begin to search again to reach and track the MPP at "10V, 1.54A, and 15.4W".

The performance of the classical PSO controller to respond and track the new MPP at PV output voltage of"10V" and current of "1.54A" takes about "1.16 sec" as shown in Figure 13 (c). On the other hand, the proposed PSO controller takes about "0.14 sec" to respond and track the new MPP as shown in Figure 13 (d).

5. Conclusions

This article produced an improved particle swarm optimization controller to insist on pursuing the photovoltaic system global maximum power point in the shortest possible time despite the surrounding climatic changes. This improved process depends on joining a powerful mechanism to the classical PSO controller performance to increase its effectiveness. By that, the exploration area limits can be retracted after each iteration by avoiding the search portions containing the weakly solutions. On the other hand, stray particles were directed to explore solutions sandwiched between the two strongest solutions that were found. The simulation results and the experimental results verified the following points. The proposed improved particle swarm optimization controller provided better response and lower convergence time than the classical controller. Moreover, it remarkably betters damping in the output power oscillations.

References

1. Gibson, T. L., & Kelly, N. A. (2008). Optimization of solar powered hydrogen production using photovoltaic electrolysis devices. International journal of hydrogen energy, 33(21), 5931-5940.
2. Kumar, N., Hussain, I., Singh, B., & Panigrahi, B. K. (2017). Peak power detection of PS solar PV panel by using WPSCO. IET Renewable Power Generation, 11(4), 480-489.
3. Irisawa, K., Saito, T., Takano, I., & Sawada, Y. (2000, September). Maximum power point tracking control of photovoltaic generation system under non-uniform insolation by means of monitoring cells. In Conference Record of the Twenty-Eighth IEEE Photovoltaic Specialists Conference-2000 (Cat. No. 00CH37036) (pp. 1707-1710). IEEE.
4. Kandemir, E., Cetin, N. S., & Borekci, S. (2017). A comprehensive overview of maximum power extraction methods for PV systems. Renewable and sustainable energy reviews, 78, 93-112.
5. Hossam-Eldin, A. A., Abdelsalam, A. K., Youssef, K. H., & Ali, E. M. (2020, December). Fast Convergence Modified Cuckoo Search Algorithm to Pursue String PV Modules Maximum Power Point under Partial Shading Conditions. In 2020 30th International Conference on Computer Theory and Applications (ICCTA) (pp. 101-107). IEEE.
6. Omar, O. A., Badra, N. M., & Attia, M. A. (2018). Enhancement of on-grid PV system under irradiance and temperature variations using new optimized adaptive controller. International Journal of Electrical and Computer Engineering (IJECE), 8(5), 2650-2660.
7. Pachaivannan, N., Subburam, R., Padmanaban, M., & Subramanian, A. (2021). Certain investigations of ANFIS assisted CPHO algorithm tuned MPPT controller for PV arrays under partial shading conditions. Journal of Ambient Intelligence and Humanized Computing, 1-16.
8. Liu, Y. H., Chen, J. H., & Huang, J. W. (2015). A review of maximum power point tracking techniques for use in partially shaded conditions. Renewable and Sustainable Energy Reviews, 41, 436-453.
9. Yang, B., Yu, T., Zhang, X., Li, H., Shu, H., Sang, Y., & Jiang, L. (2019). Dynamic leader based collective intelligence for maximum power point tracking of PV systems affected by partial shading condition. Energy Conversion and Management, 179, 286-303.
10. Yang, B., Yu, T., Zhang, X., Li, H., Shu, H., Sang, Y., & Jiang, L. (2019). Dynamic leader based collective intelligence for maximum power point tracking of PV systems affected by partial shading condition. Energy Conversion and Management, 179, 286-303.
11. Eltamaly, A. M., Farh, H. M., & Al-Saud, M. S. (2019). Grade point average assessment for metaheuristic GMPP techniques of partial shaded PV systems. IET Renewable Power Generation, 13(8), 1215-1231.
12. Li, H., Yang, D., Su, W., Lü, J., & Yu, X. (2018). An overall distribution particle swarm optimization MPPT algorithm for photovoltaic system under partial shading. IEEE Transactions on Industrial Electronics, 66(1), 265-275.
13. Zhao, Z., Cheng, R., Yan, B., Zhang, J., Zhang, Z., Zhang, M., & Lai, L. L. (2020). A dynamic particles MPPT method for photovoltaic systems under partial shading conditions. Energy Conversion and Management, 220, 113070.
14. Chauhan, U., Singh, V., Kumar, B., & Rani, A. (2020). An improved MVO assisted global MPPT algorithm for partially shaded PV system. Journal of Intelligent & Fuzzy Systems, 38(5), 6715-6726.
15. Li, H., Yang, D., Su, W., Lü, J., & Yu, X. (2018). An overall distribution particle swarm optimization MPPT algorithm for photovoltaic system under partial shading. IEEE Transactions on Industrial Electronics, 66(1), 265-275.
16. Sharma, S., Jain, K. K., & Sharma, A. (2015). Solar cells: in research and applications—a review. Materials Sciences and Applications, 6(12), 1145.
17. Vieira, R. G., de Araújo, F. M., Dhimish, M., & Guerra, M. I. (2020). A comprehensive review on bypass diode application on photovoltaic modules. Energies, 13(10), 2472.

18. Ali, E. M., Hossam-Eldin, A. A., & Abdelsalam, A. K. (2021, July). An Enhanced Particle Swarm Optimization Algorithm Fitting for Photovoltaic Max Power Tracking under Different Climatic Conditions. In 2021 International Telecommunications Conference (ITC-Egypt) (pp. 1-4). IEEE.
19. Ali, E. M., Abdelsalam, A. K., Youssef, K. H., & Hossam-Eldin, A. A. (2021). An Enhanced Cuckoo Search Algorithm Fitting for Photovoltaic Systems' Global Maximum Power Point Tracking under Partial Shading Conditions. Energies, 14(21), 7210.
20. Yu, Y. F., Li, G., & Xu, C. (2013). An improved particle swarm optimization algorithm. In Applied Mechanics and Materials (Vol. 401, pp. 1328-1335). Trans Tech Publications Ltd.
21. Bai, Q. (2010). Analysis of particle swarm optimization algorithm. Computer and information science, 3(1), 180.
22. Ouali, M. A., Ghanai, M., & Chafaa, K. (2018). A new type-2 fuzzy modelling and identification for electrophysiological signals: a comparison between PSO, BBO, FA and GA approaches. International Journal of Modelling, Identification and Control, 29(2), 163-184.
23. Zakzouk, N. E., Elsaharty, M. A., Abdelsalam, A. K., and Helal, A. A., "Improved performance low-cost incremental conductance PV MPPT technique," IET Renewable Power Generation, vol. 10, no. 4, pp. 561-574, 2016.